



## Article

# Identifying Structural Features of Nucleotide Analogues to Overcome SARS-CoV-2 Exonuclease Activity

Xuanting Wang <sup>1,2</sup> , Chuanjuan Tao <sup>1,2</sup>, Irina Morozova <sup>1,2</sup>, Sergey Kalachikov <sup>1,2</sup>, Xiaoxu Li <sup>1,2</sup>, Shiv Kumar <sup>1,2</sup>, James J. Russo <sup>1,2</sup> and Jingyue Ju <sup>1,2,3,\*</sup> 

<sup>1</sup> Center for Genome Technology and Biomolecular Engineering, Columbia University, New York, NY 10027, USA; xw2467@columbia.edu (X.W.); ct2439@columbia.edu (C.T.); im198@columbia.edu (I.M.); sk363@columbia.edu (S.K.); lx2109@columbia.edu (X.L.); sk3765@columbia.edu (S.K.); jjr4@columbia.edu (J.J.R.)

<sup>2</sup> Department of Chemical Engineering, Columbia University, New York, NY 10027, USA

<sup>3</sup> Department of Molecular Pharmacology and Therapeutics, Columbia University, New York, NY 10032, USA

\* Correspondence: dj222@columbia.edu

**Abstract:** With the recent global spread of new SARS-CoV-2 variants, there remains an urgent need to develop effective and variant-resistant oral drugs. Recently, we reported in vitro results validating the use of combination drugs targeting both the SARS-CoV-2 RNA-dependent RNA polymerase (RdRp) and proofreading exonuclease (ExoN) as potential COVID-19 therapeutics. For the nucleotide analogues to be efficient SARS-CoV-2 inhibitors, two properties are required: efficient incorporation by RdRp and substantial resistance to excision by ExoN. Here, we have selected and evaluated nucleotide analogues with a variety of structural features for resistance to ExoN removal when they are attached at the 3' RNA terminus. We found that dideoxynucleotides and other nucleotides lacking both 2'- and 3'-OH groups were most resistant to ExoN excision, whereas those possessing both 2'- and 3'-OH groups were efficiently removed. We also found that the 3'-OH group in the nucleotide analogues was more critical than the 2'-OH for excision by ExoN. Since the functionally important sequences in Nsp14/10 are highly conserved among all SARS-CoV-2 variants, these identified structural features of nucleotide analogues offer invaluable insights for designing effective RdRp inhibitors that can be simultaneously efficiently incorporated by the RdRp and substantially resist ExoN excision. Such newly developed RdRp terminators would be good candidates to evaluate their ability to inhibit SARS-CoV-2 in cell culture and animal models, perhaps combined with additional exonuclease inhibitors to increase their overall effectiveness.

**Keywords:** SARS-CoV-2; coronaviruses; antivirals; RNA-dependent RNA polymerase; exonuclease; nucleotide analogues



**Citation:** Wang, X.; Tao, C.; Morozova, I.; Kalachikov, S.; Li, X.; Kumar, S.; Russo, J.J.; Ju, J. Identifying Structural Features of Nucleotide Analogues to Overcome SARS-CoV-2 Exonuclease Activity. *Viruses* **2022**, *14*, 1413. <https://doi.org/10.3390/v14071413>

Academic Editors: Zhengqiang Wang and Robert J. Geraghty

Received: 2 June 2022

Accepted: 25 June 2022

Published: 28 June 2022

**Publisher's Note:** MDPI stays neutral with regard to jurisdictional claims in published maps and institutional affiliations.



**Copyright:** © 2022 by the authors. Licensee MDPI, Basel, Switzerland. This article is an open access article distributed under the terms and conditions of the Creative Commons Attribution (CC BY) license (<https://creativecommons.org/licenses/by/4.0/>).

## 1. Introduction

SARS-CoV-2, the causative agent of COVID-19, is a member of the Nidovirales order of positive-strand RNA viruses [1]. Members of this coronavirus family include those responsible for SARS, MERS and assorted mild respiratory infections in humans and animals [2]. The coronaviruses fall into four major groups, designated alpha, beta, gamma and delta [3]; SARS-CoV, MERS-CoV and SARS-CoV-2 are in the beta lineage and are closely related to one another [4]. Like other coronaviruses, SARS-CoV-2 has a large RNA genome encoding more than 25 proteins. There are 16 nonstructural proteins (Nsp1-16), many of which form the replication-transcription complex (RTC). The functions of these proteins have been extensively reviewed [5,6], and several of them have been selected as targets for drug development.

Because of the large genome size of the coronaviruses (>30 kb), their relatively low fidelity RNA-dependent RNA polymerase (RdRp) would tend to produce a high number of errors during RNA replication and transcription [7]; the resulting mutations could

impede viral replication and infectivity. To overcome this, the coronaviruses possess a 3'-5' exonuclease (ExoN), consisting of Nsp14 and Nsp10, involved in proofreading and error repair [7–17], along with other functions such as evasion of host immunity [18]. The RdRp and ExoN of SARS-CoV-2 work together in lockstep to ensure that mismatches and modified nucleotides mistakenly incorporated by the RdRp are efficiently removed by ExoN, and ExoN knockout mutants of SARS-CoV-2 are nonviable [14].

The complete structure of the RTC (Nsp12/7/8, Nsp14/10, Nsp13 helicase, and associated proteins Nsp9 and Nsp16), as well as that of the individual components of the complex, has been resolved by cryo-electron microscopy and X-ray crystallography in order to determine which sites in these proteins are critical for protein-protein interactions or catalytic activity. The structures determined include the replicating RdRp complex in the absence and presence of RNA and specific nucleotide inhibitors [19–24]; the ExoN complex, including in the presence of mismatched bases, implicating a variety of proofreading mechanisms including backtracking [11,25]; and the complete and near-complete RTC that includes helicase and capping enzymes [26–30].

The Nsp14 protein contains an ExoN functional domain that provides replication and transcription error correction, allowing SARS-CoV-2 to maintain its large-sized genome [12,31–34]. Enzymatic assays confirm that the accessory protein Nsp10 stabilizes substrate binding by ExoN to support its exoribonuclease activity [13]. The Nsp14 and Nsp10 residues involved in these interactions have been studied using 3D structure analysis and artificial mutagenesis. Artificial mutations introduced into Nsp14 helped identify the positions most important for its function [12,35,36]. Specific residues were identified in SARS-CoV that might be targeted for preventing Nsp14-Nsp10 interactions and activity, with possible negative consequences for viral replication [37,38]. The activity of Nsp14 has recently been reported to be enhanced by Nsp8 [7].

Recently, various assays have been described to measure the SARS-CoV-2 ExoN activity [7,15,39,40]. Based on molecular assays with reconstituted enzyme complexes (Nsp14/Nsp10), the ExoN enzyme can recognize and remove mismatches at the 3' end as well as internally, the latter suggesting an endonuclease-based repair mechanism distinct from that of the Nsp15 endonuclease [7]. Moreover, Nsp14 can excise not only mismatched natural bases but a wide variety of nucleotide analogues that are incorporated into the RNA [7]. Thus, we and others have reasoned that the well-choreographed dance between the RdRp and the ExoN represents an Achilles' heel for the virus: if we can take advantage of the low fidelity of the RdRp to incorporate modified nucleotides that terminate the RNA polymerase reaction, and at the same time, prevent the removal of these nucleotide analogues by inhibiting the ExoN, we might effectively block SARS-CoV-2 replication [7,39,41].

Drugs that are based on nucleoside and nucleotide analogues that inhibit the coronavirus RdRp (Nsp12, Nsp7 and Nsp8) and ExoN (Nsp14 and Nsp10) fall into multiple categories with respect to their modes of action. Several active forms of nucleoside/nucleotide analogues can be incorporated into the viral RNA by the RdRp where they terminate further incorporation or they lead to mutations in the RNA, either of which may impede various aspects of the viral life cycle [39,42–47]. However, if they are efficiently excised by ExoN, their effects may be abrogated. For the drug to be effective, its rate of incorporation must significantly exceed its rate of excision, the incorporated nucleotide must be resistant to ExoN, or the ExoN must itself be inhibited by an exonuclease inhibitor [16,41,47,48]. Alternative non-nucleotide-based inhibitors of the RdRp have also been explored as a strategy for interfering with SARS-CoV-2 replication [49,50]. Since these non-nucleotide inhibitors are not incorporated into RNA, they would not be affected by the ExoN excision mechanism.

Previously, we demonstrated that the triphosphate forms of numerous nucleotide analogues, including FDA-approved drugs for other viral infections, are capable of being incorporated into RNA by the SARS-CoV-2 RdRp complex and of terminating RNA extension with varying efficiency, in either immediate or delayed fashion [46,47]. Minskaia et al. [51] reported that the SARS-CoV ExoN did not hydrolyze DNA or ribose-2'-O-methylated

RNA substrates. We identified several hepatitis C virus (HCV) NS5A inhibitors [52] that also inhibited the SARS-CoV-2 exonuclease [41,53,54]. Several of these ExoN inhibitors acted synergistically with RdRp inhibitors in blocking viral replication in Calu-3 cells [41]; recently, other investigators have proposed similar combination drug approaches [55,56]. Interestingly, our studies indicated that the HCV NS5A inhibitors Velpatasvir and Dacatasvir not only inhibited the exonuclease but inhibited RdRp activity as well [53,54]. We also noticed that Tenofovir, once incorporated into RNA by RdRp, was largely resistant to removal by ExoN [41]. This led us to examine further the properties of nucleotide analogues that might lead to such ExoN resistance.

In this paper, based on published sequence information, we first assess the conservation of protein sequences within the exonuclease functional sites of Nsp14 and Nsp10 in SARS-CoV-2 variants (Figure 1 and Figure S1). The high conservation observed for these proteins indicates that inhibitors of ExoN function would be effective against current and future variants of SARS-CoV-2. Second, we present the results of enzymatic assays evaluating the ability of nucleotide analogues with various structural features to be excised from the 3' end of RNA by ExoN. We focus on nucleotides and nucleotide analogues with sugar modifications, such as lack of the 2'-OH, lack of the 3'-OH, or lack of both 2'- and 3'-OH, as well as base-modified nucleotides. Among the molecules we tested, nucleotide analogues lacking both the 2'- and 3'-OH moieties were most resistant to ExoN activity. Given the sequence conservation of Nsp14/10 among SARS-CoV-2 variants, the structural features of nucleotide analogues identified above can guide the design and synthesis of novel RdRp inhibitors that can both be efficiently incorporated by the RdRp and substantially resist ExoN excision, perhaps combined with additional exonuclease inhibitors to increase their overall effectiveness to inhibit SARS-CoV-2.

## 2. Materials and Methods

Nucleoside triphosphate analogues were purchased from TriLink BioTechnologies (Cidofovir-DP, 2'-NH<sub>2</sub>-dUTP, Cordycepin-TP, ddATP, ddCTP, ddGTP, Biotin-16-dUTP), Invitrogen (Biotin-16-UTP), Santa Cruz Biotechnology (Stavudine-TP), Amersham Life Sciences (Zidovudine-TP) or Alfa Chemistry (Tenofovir-DP). RNA oligonucleotides (template-loop-primers) were purchased from Dharmacon. HIV reverse transcriptase, SuperScript IV reverse transcriptase and T7 RNA polymerase were purchased from Millipore Sigma, Thermo Fisher and New England BioLabs, respectively. The expression and purification of the SARS-CoV-2 exonuclease Nsp14/Nsp10 complex have been described in our previous study [41].

### 2.1. Extension Reactions with Reverse Transcriptase to Produce Nucleotide Analogue-Extended RNA

The RNA template-loop-primers (5'-UUUUCUACGCGUAGUUUUCUACGCG-3' for Biotin-16-dUTP, Stavudine-TP or Zidovudine-TP extension reactions; 5'-UUUUCACCGCGUAGUUUUCUACGCG-3' for ddGTP extension reactions; 5'-UUUUCAUCGCGUAGUUUUCUACGCG-3' for Tenofovir-DP or ddATP extension reactions; 5'-UUUUCUGCGCGUAGUUUUCUACGCG-3' for Cidofovir-DP or ddCTP) were annealed by heating to 75 °C for 3 min and cooling to room temperature in 1 × HIV reverse transcriptase (RT) or 1 × SuperScript IV RT reaction buffer. Then, 10 µL of the appropriate annealed RNA template-loop-primer solution (10 µM) was added to 8 µL of the reverse transcriptase solution consisting of 54.4 U of HIV RT or 200 U of SuperScript IV RT in 1 × appropriate buffer. Finally, 2 µL of a solution containing 10 mM Biotin-16-dUTP, Stavudine-TP, Cidofovir-DP, Tenofovir-DP, Zidovudine-TP, ddATP, ddCTP or ddGTP was added and incubation was carried out for 4 h at 45 °C. The 20 µL extension reactions contained 54.4 U HIV RT or 200 U SuperScript IV RT, 5 µM RNA template-loop-primer, and 1 mM Biotin-16-dUTP, Stavudine-TP, Cidofovir-DP, Tenofovir-DP, Zidovudine-TP, ddATP, ddCTP or ddGTP. The 1 × HIV RT reaction buffer contained 10 mM Tris-HCl pH 8, 10 mM KCl, 2 mM MgCl<sub>2</sub> and 1 mM β-mercaptoethanol. Desalting of the reaction mixture was performed with an

Oligo Clean & Concentrator kit (Zymo Research), resulting in ~10 µL purified aqueous RNA solutions. Then, 1 µL of each solution was subjected to MALDI-TOF MS (Bruker ultrafleXtreme) analysis. The remaining ~9 µL RNA extension products were used to test exonuclease activity.

### 2.2. Extension Reactions with RNA Polymerase to Produce Nucleotide Analogue-Extended RNA

The RNA template-loop-primers (5'-UUUUCUACGCGUAGUUUUCUACGCG-3' for 2'-NH<sub>2</sub>-dUTP and Biotin-16-UTP; 5'-UUUUCAUCGCGUAGUUUUCUACGCG-3' for Cordycepin-TP) were annealed by heating to 75 °C for 3 min and cooling to room temperature in 1 × RNA Pol buffer. Then, 10 µL of the appropriate annealed RNA template-loop-primer solution (10 µM) was added to 8 µL of an RNA polymerase solution consisting of 400 U of T7 RNA polymerase in 1 × RNA Pol buffer. Finally, 2 µL of a solution containing 10 mM of 2'-NH<sub>2</sub>-dUTP, Biotin-16-UTP or Cordycepin-TP was added and incubated for 4 h at 37 °C. The 20 µL extension reactions contained 400 U T7 RNA polymerase, 5 µM RNA template-loop-primer, and 1 mM 2'-NH<sub>2</sub>-dUTP, Biotin-16-UTP or Cordycepin-TP. The 1 × RNA polymerase reaction buffer contains 40 mM Tris-HCl, 6 mM MgCl<sub>2</sub>, 1 mM DTT and 2 mM spermidine. Desalting of the reaction mixture was performed with an Oligo Clean & Concentrator kit (Zymo Research), resulting in ~10 µL purified aqueous RNA solutions. Then, 1 µL of each solution was subjected to MALDI-TOF MS (Bruker ultrafleXtreme) analysis. The remaining ~9 µL RNA extension products were used to test exonuclease activity.

### 2.3. Exonuclease Reactions with SARS-CoV-2 Nsp14/Nsp10 Complex

The synthetic RNA template-loop-primers with A, U, G, C, dC, 2'-F-dC or 2'-OMe-C at the 3' terminus (sequences shown in Figures 2b,3b, 4b and S4b,e,h,k respectively) or the extended template-loop-primers with Biotin-16-U, Biotin-16-dU, Stavudine, Cidofovir, Tenofovir, Zidovudine, 2'-NH<sub>2</sub>-dU, Cordycepin, ddA, ddC or ddG at the 3' end were annealed by heating to 75 °C for 3 min and cooling to room temperature in 1 × exonuclease reaction buffer. To the 10 µL annealed extended RNA template-loop-primer solution (1 µM), 10 µL of exonuclease Nsp14/10 complex (100 nM) in 1 × exonuclease reaction buffer was added and incubated at 37 °C for 5, 10 or 15 min. The final concentrations of reagents in the 20 µL reactions were 50 nM Nsp14/10 and 500 nM different RNAs. The 1 × exonuclease reaction buffer contains 40 mM Tris-HCl pH 8, 1.5 mM MgCl<sub>2</sub>, and 5 mM DTT. After incubation, each reaction was quenched by the addition of 2.2 µL of an aqueous solution of EDTA (100 mM). Following desalting using an Oligo Clean & Concentrator (Zymo Research), the samples were subjected to MALDI-TOF MS (Bruker ultrafleXtreme) analysis.

## 3. Results and Discussion

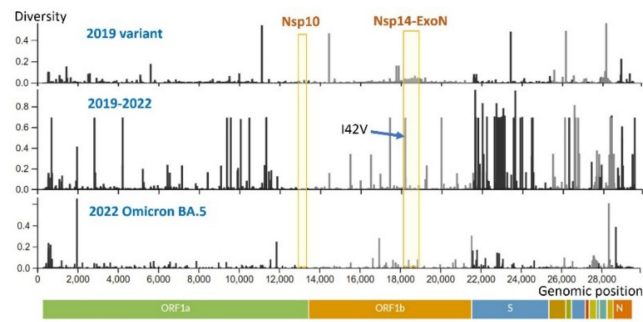
### 3.1. Sequence Conservation in Nsp14 and Nsp10

With more than 5 million genomes of SARS-CoV-2 sequenced, naturally occurring mutations have been analyzed in a number of strains, including the most recent variants of concern to public health [57–59]. Overall, SARS-CoV-2 is a relatively conservative virus compared to other RNA viruses [60]. This low genomic variability means that coronaviral genomes contain lower numbers of mutations, and analysis of those mutations that become widespread may help in our understanding of viral functions. In the coronaviruses, low genome variability is ensured by the activity of ExoN during RNA replication [7,9,11,12,14,15].

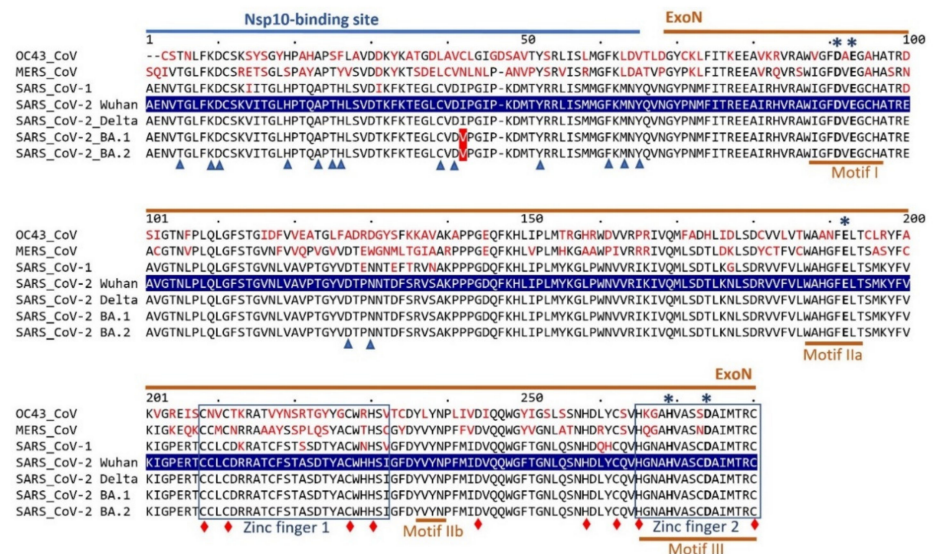
The majority of genomic sequence variations observed in SARS-CoV-2 variants are located within genes encoding Spike, structural and accessory proteins, while the members of the ExoN complex, Nsp14 and Nsp10 genes, accumulate fewer nucleotide changes, most of which are synonymous (not causing changes in the encoded amino acids). Figure 1a shows amino acid diversity profiles for an early 2019 SARS-CoV-2 strain and the recent Omicron BA.5 variant. Nsp10 displays high sequence conservation. Moving from early variants to more recent ones, the overall amino acid diversity in Nsp14 becomes lower, in high contrast with the increasing sequence diversity in the Spike protein, for example. Within the ExoN-related portion of Nsp14, only one amino acid position retains diversity, displaying a conservative substitution I42V. Such sequence conservation in Nsp14 and Nsp10 may reflect a negative evolutionary pressure on the structure of the protein components of the ExoN complex, preserving its function, along with a bottleneck effect accounting for the widespread distribution of the neutral I42V.

Figure 1b shows the primary structure of the exonuclease-related domains of the Nsp14 protein, in four SARS-CoV-2 strains (the original 2019 isolate Wuhan-Hu-1, Delta, Omicron BA.1 and Omicron BA.2), along with SARS-CoV-1, MERS-CoV and OC43-CoV, a coronavirus causing the common cold. Positions marked with asterisks, triangles and diamonds in Figure 1b correspond to amino acid residues that are critical for ExoN function. Artificially introduced mutations at these positions have been shown to hinder the ExoN proofreading activity [12,14,36]. The catalytic residues at positions marked with asterisks comprise the active center of the ExoN domain of Nsp14.

When recent variants of SARS-CoV-2 are compared to the original 2019 strain, very few mutations in the replication component, including Nsp14 and Nsp10 proteins, became fixed in the population. Within the portion of Nsp14 that spans the Nsp10-binding site and ExoN domain (Figure 1b), the only widespread naturally occurring mutation is I42V, a conservative substitution in the Nsp10-binding site, as evidenced by analysis of more than 80,000 SARS-CoV-2 genomes [59]. This is the only mutation that is ubiquitous in the exonuclease-related portion of Nsp14 in Omicron sub-lineages [60]. Another amino acid change in Nsp14, a D to N substitution at amino acid position 212 in the Figure 1b alignment (mutation not shown), present in some BA.2 sequences (e.g., GenBank accession ON117774), is located in the first zinc finger region of the ExoN domain. This substitution is between similar polar amino acids, aspartic acid and asparagine, and it does not hit any position that has been shown to be important for zinc finger formation. Eskier et al. [34] reported that a non-synonymous substitution F234L (position according to Figure 1b, mutation not shown), identified based on analysis of ~30,000 SARS-CoV-2 genomes and located within the Nsp14 zinc finger 1, was associated with an increased genome-wide mutational load, but so were the other two identified nucleotide substitutions that were synonymous and therefore not affecting the corresponding protein sequence.



(a)



(b)

**Figure 1. (a) Diversity of the encoded amino acids along genomic sequences of SARS-CoV-2.** Profiles for three genomic sets are shown—**top**: diversity within ~2000 genomic sequences of the early SARS-CoV-2 sampled between December 2019 and March 2020; **middle**: diversity within ~2000 genomes collected in December 2019–May 2022; **bottom**: diversity within ~900 genomes of the recent Omicron BA.5 variant collected from January–May of 2022. The Nsp14-ExoN boundaries include only the first 280 aa positions involved in ExoN function (the same region shown in the sequence alignment). The arrow points to the position of the ubiquitous I42V aa substitution in Nsp14. Profiles are constructed by the Nextstrain webtool using genomic sequences from GISAID (<https://www.gisaid.org/>; Nextstrain datasets: “early-19A” and “22B Omicron”; webtool accessed on 25 May 2022 at <https://nextstrain.org> [61]). **(b) Protein sequence conservation in the ExoN domain of Nsp14 in representative beta Coronaviridae strains.** Partial Nsp14 protein alignment spans the Nsp10-binding site (amino acid positions 1–64) and the adjacent ExoN domain (aa positions 68–280). Nsp14 of the SARS-CoV-2 Wuhan-Hu-1 variant (highlighted in blue) was used as a reference: amino acid differences in other variants compared to the reference sequence are shown in red. Functional motifs comprising the ExoN active site are underlined, and the zinc finger regions are boxed [12,14,36]. ExoN catalytic residues are indicated with asterisks; residues interacting with Nsp10 are marked by blue triangles; and positions critical for zinc fingers, protein solubility or ExoN activity are shown as red diamonds [12,14]. The sequences were retrieved from GenBank: OC43-CoV (common cold; accession number YP\_009924328), MERS-CoV (YP\_009047225), SARS-CoV-1 (JX163928), and variants of SARS-CoV-2: Wuhan-Hu-1 (YP\_009725309, original strain isolated in 2019), Delta (OM990852), and Omicron BA.1 (ON141240) and BA.2 (ON553707). Protein alignment was built using Clustal Omega [62,63], visualized by MView [63,64], and then annotated.

In the relatively short and conservative Nsp10 protein of SARS-CoV-2, naturally occurring mutations are rare (Figure S1). Artificially introduced mutations in many of the evolutionarily highly conserved amino acid positions in Nsp10 have been shown to lead to reduced fidelity [65] or even be lethal to coronaviruses by interfering with viral replication [8,37]. A naturally occurring amino acid substitution R134N, detected by analysis of ~1000 genomes of SARS-CoV-2 B.1.617, is neutral and not under selective pressure [58].

Based on the conservative nature of components of the ExoN complex, we predict that any inhibitor for this enzymatic function should have broad-spectrum inhibitory potential for most current and possibly future strains of SARS-CoV-2.

### 3.2. Excision of Nucleotide Analogues from RNA by SARS-CoV-2 ExoN

In our previous study, we reported that Tenofovir-terminated RNA showed high resistance toward excision by the SARS-CoV-2 ExoN compared to RNA terminated with Remdesivir, Molnupiravir, Sofosbuvir or Favipiravir at the 3' end [41]. We also demonstrated that the triphosphate forms of numerous nucleotide analogues with different structural features can be incorporated into RNA by the SARS-CoV-2 RdRp complex and terminate RNA extension with varying efficiency in either immediate or delayed fashion [46,47]. Here, with the goal of providing insights into the design of viral polymerase inhibitors that could evade the exonuclease proofreading function, we systematically investigated the chemical or structural properties of selected nucleotide analogues for exonuclease excision.

We focus on nucleotides and nucleotide analogues with sugar modifications, such as lack of the 2'-OH, lack of the 3'-OH, or lack of both 2'- and 3'-OH, as well as base-modified nucleotides. The nucleotide analogues lacking the 2'-OH group include 2'-deoxycytosine-5'-triphosphate (2'-dCTP), 2'-fluoro-2'-deoxycytosine-5'-triphosphate (2'-F-dCTP), 2'-O-methylcytosine-5'-triphosphate (2'-OME-CTP) and 2'-amino-2'-deoxyuridine-5'-triphosphate (2'-NH<sub>2</sub>-2'-dUTP). Two nucleotide analogues lacking a 3'-OH group, Cordycepin-5'-triphosphate (3'-dATP) and the acyclic nucleotide analogue Cidofovir diphosphate (Cid-DP), were evaluated. We also investigated nucleotide analogues lacking both 2'- and 3'-OH groups: the dideoxynucleoside-5'-triphosphates (ddATP, ddCTP and ddGTP), a ddUTP derivative (Stavudine-5'-triphosphate, Sta-TP), Zidovudine-5'-triphosphate (AZT-TP), as well as another acyclic nucleotide analogue, Tenofovir diphosphate (Tfv-DP). Two nucleotides with modifications at the 5-position of uridine were investigated, biotin-16-aminoallyl-2'-deoxyuridine-5'-triphosphate (Biotin-16-dUTP) and biotin-16-aminoallyl-uridine-5'-triphosphate (Biotin-16-UTP). Cordycepin (3'-deoxyadenosine) has been shown to have biological activities in a wide variety of disease processes [66] but displays some toxicity due to off-target effects on mitochondrial RNA polymerases [67]. We synthesized template-loop-primers with the different nucleotide analogues mentioned above at their 3' ends to perform the following exonuclease assays.

As shown in Figure 2, adenosine- (a), Cordycepin- (d), dideoxyadenosine- (g) or Tenofovir-terminated RNA (j) were separately incubated with the SARS-CoV-2 pre-assembled exonuclease complex (Nsp14/Nsp10) at 37 °C for 0 and 10 min, and the results were analyzed by MALDI-TOF mass spectrometry. The spectra in the middle (Figure 2b,e,h,k) reflected the molecular weights of the corresponding intact RNAs. After 10 min of exonuclease treatment, the RNA products were re-analyzed by MS, and the results are shown in Figure 2c,f,i,l. As an example, the peak at 8168 Da corresponds to the Cordycepin-terminated RNA before exonuclease treatment (Figure 2e). Exonuclease activity caused nucleotide cleavage from the 3'-end of the Cordycepin-terminated RNA, as shown by the eight lower molecular weight fragments corresponding to cleavage of 5–13 nucleotides (Figure 2f), with about 10% intact RNA remaining (peak at 8175 Da), indicating some level of ExoN resistance. Similarly, ddA- and Tenofovir-terminated RNAs were analyzed before (Figure 2h,k) and after ExoN treatment (Figure 2i,l). Approximately 60% and 55% of intact RNAs were observed, respectively (Figure 2i,l), indicating that both nucleotide analogues have substantial ExoN resistance. As a control, the intact adenosine-terminated RNA peak (around 8183 Da, Figure 2b) was not

observed after treatment (Figure 2c), indicating that the natural nucleotide A is completely removed by the Nsp14/10 complex. By comparing spectra (Figure 2c,f,i,l), we concluded that ddA- and Tenofovir-terminated RNAs exhibit high resistance toward ExoN cleavage while Cordycepin-terminated RNA displays moderate resistance.

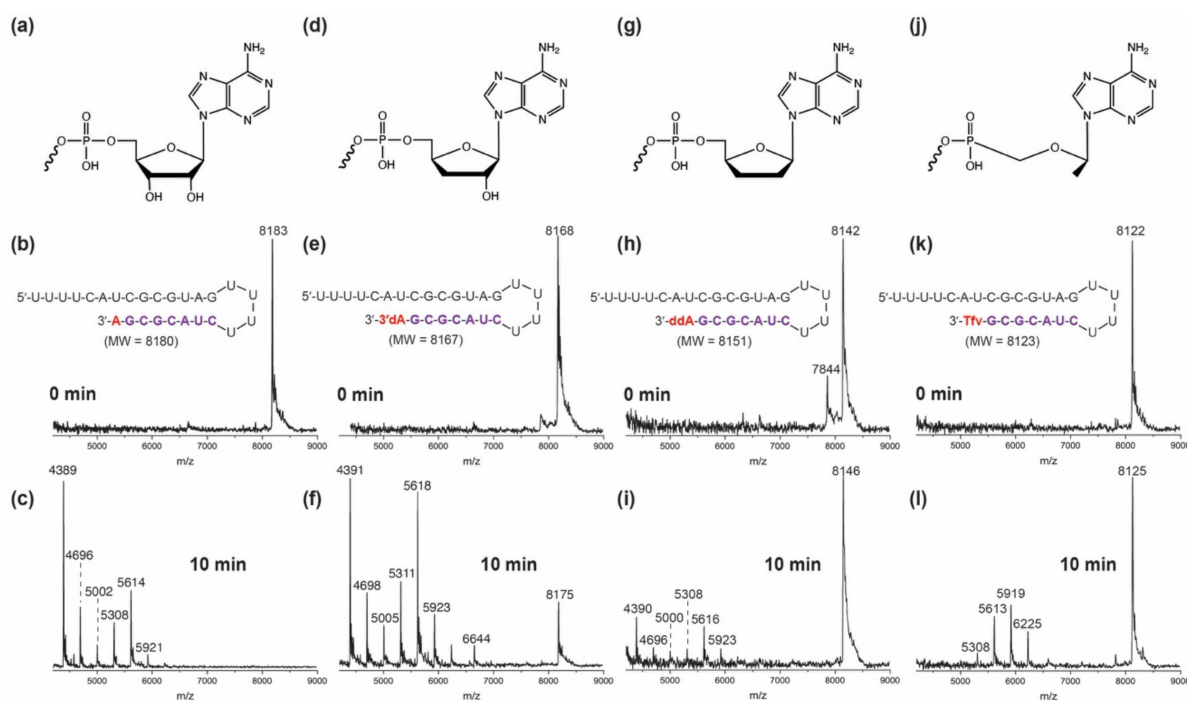


**Figure 2.** SARS-CoV-2 exonuclease activity with adenosine- or adenosine analogue-terminated RNA. A mixture of 500 nM template-loop-primer terminated at its 3' end with either A (a), Cordycepin (d), ddA (g) or Tenofovir (TfV) (j) (sequences shown in b,e,h,k) and SARS-CoV-2 pre-assembled exonuclease complex (Nsp14/Nsp10) was incubated at 37 °C for 10 min. These intact RNAs (b,e,h,k) and their respective exonuclease reaction products (c,f,i,l) were analyzed by MALDI-TOF MS. The signal intensity was normalized to the highest peak. The accuracy for  $m/z$  determination is approximately  $\pm 10$  Da.

A previous study suggested that 3'-deoxynucleotide analogues could potentially resist exonuclease excision [11]. Moreover, 3'-deoxyadenosine-5'-triphosphate (Cordycepin TP) has been demonstrated to be incorporated efficiently and terminate RNA synthesis by the SARS-CoV-2 RdRp [66]. To confirm whether 3'-dA can evade exonuclease activity, the exonuclease resistance of Cordycepin-terminated RNA was further evaluated at different incubation times. Adenosine- and Cordycepin-terminated RNAs were treated with exonuclease for 0, 5, 10 or 15 min (Figure S2). As incubation time increases, a reduced amount of the Cordycepin-extended intact RNA peak (at ~8168 Da) is observed, while the 14 nucleotide-long RNA fragment peak (at ~4388 Da) becomes increasingly dominant (Figure S2g–j). In contrast, adenosine-terminated RNA was rapidly degraded by exonuclease (Figure S2c–e). Thus, this result indicates that 3'-dA only has some resistance to ExoN.

Figures 3 and S3 present the SARS-CoV-2 exonuclease results for uridine- and uridine analogue-terminated RNAs. The MALDI-TOF MS spectra of RNAs extended with 2'-NH<sub>2</sub>-2'-dUTP, Zidovudine-TP, Stavudine-TP, Biotin-16-UTP and Biotin-16-dUTP are shown in Figures 3e,h,k and S3b,e. After incubation with the SARS-CoV-2 Nsp14/10 complex, only Zidovudine- and Stavudine-terminated RNAs retain ~40% and 50% of their respective intact RNA peaks (Figure 3i,l). These results indicate that Zidovudine- and Stavudine-terminated RNAs have substantial exonuclease resistance. In the control spectrum of exonuclease-treated uridine-extended RNA (Figure 3c), no intact RNA was observed, with



the majority of fragments being 14–15 nucleotides long, indicated by the major peaks at 4411 Da and 4718 Da. After treatment with ExoN, the intact peak for the 2'-NH<sub>2</sub>-2'-dU-terminated RNA is eliminated, with mainly fragments of 18–21 nucleotides remaining (Figure 3f), indicating very low resistance to ExoN. The Biotin-16-U- and Biotin-16-dU-terminated RNAs (Figure S3c,f) also displayed very low resistance toward ExoN activity, with the intact RNA peak completely eliminated, with predominantly 18–21 nucleotide long fragments remaining.

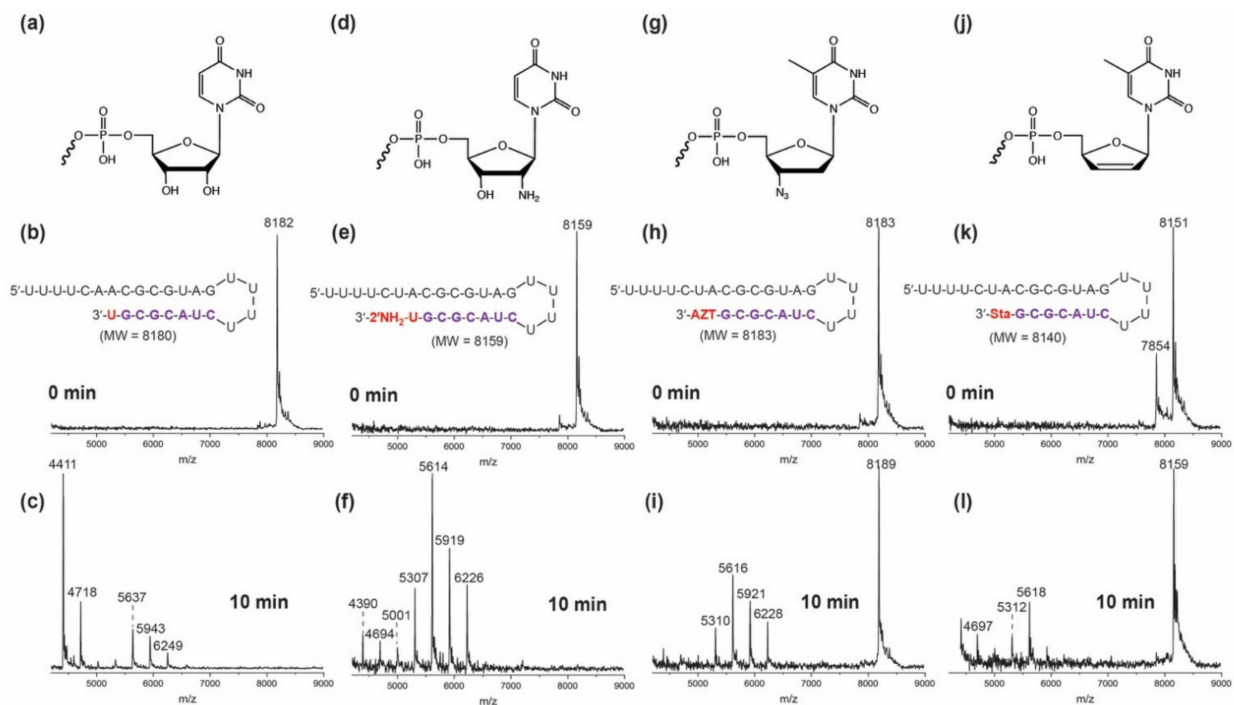


**Figure 3.** SARS-CoV-2 exonuclease activity with uridine- or uridine-analogue terminated RNA. A mixture of 500 nM template-loop-primer terminated at its 3' end with either U (a), 2'-NH<sub>2</sub>-U (d), Zidovudine (AZT) (g) or Stavudine (Sta) (j) (sequences shown in b,e,h,k) and SARS-CoV-2 pre-assembled exonuclease complex (Nsp14/Nsp10) was incubated at 37 °C for 10 min. These intact RNAs (b,e,h,k) and their respective exonuclease reaction products (c,f,i,l) were analyzed by MALDI-TOF MS. The signal intensity was normalized to the highest peak.

The results for guanosine-, ddG-, Cidofovir- and ddC-terminated RNAs are shown in Figure 4. In the presence of SARS-CoV-2 ExoN, ddG-terminated RNA shows the most ExoN resistance with predominantly the intact RNA peak (8167 Da) remaining (Figure 4f). The ddC-terminated RNA displayed a substantial level of ExoN resistance but less than ddG, as indicated by the amount of intact RNA (8147 Da) remaining (Figure 4l). Cidofovir-terminated RNA had moderate resistance to ExoN excision, with even less of the intact RNA peak (8141 Da) remaining (Figure 4i). As expected, the control G-terminated RNA was completely digested by ExoN (Figure 4c).

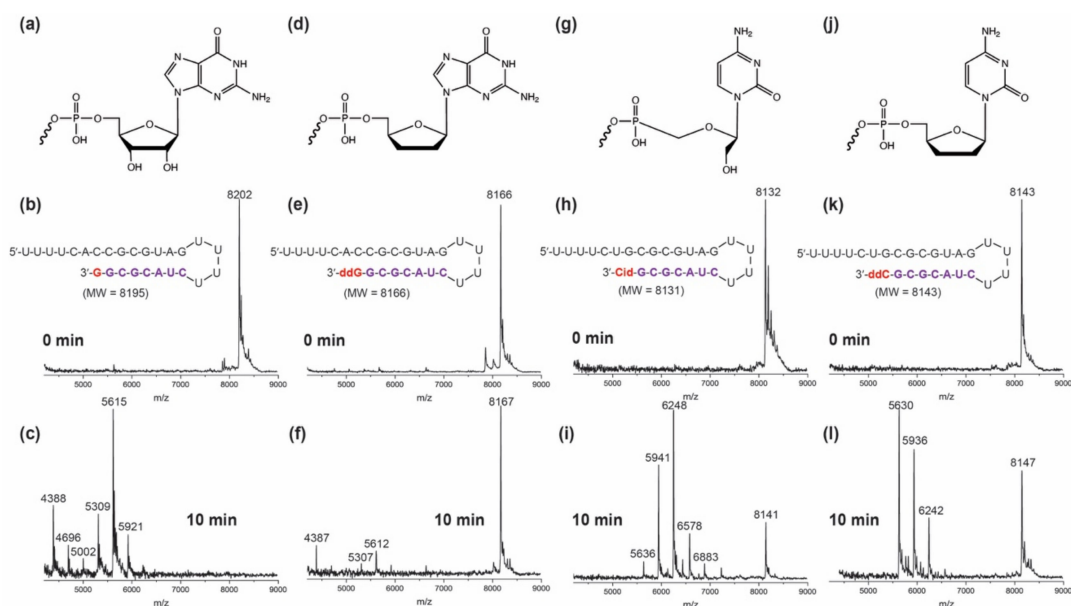


**Figure 4.** SARS-CoV-2 exonuclease activity with guanosine- or guanosine analogue-terminated RNA (a–f) and cytosine analogue-terminated RNA (g–l). A mixture of 500 nM of template-loop-primer terminated at its 3' end with either G (a), ddG (d), Cidofovir (Cid) (g) or ddC (j) (sequences shown in b,e,h,k) and SARS-CoV-2 pre-assembled exonuclease complex (Nsp14/Nsp10) was incubated at 37 °C for 10 min. These intact RNAs (b,e,h,k) and their respective exonuclease reaction products (c,f,i,l) were analyzed by MALDI-TOF MS. The signal intensity was normalized to the highest peak.

The results for RNAs terminated with cytosine and three additional cytosine analogue-terminated synthetic RNAs were treated with SARS-CoV-2 exonuclease and are depicted in Figure S4. After treatment with ExoN for 10 min, the intact RNA peaks measured at time 0 (Figure S4e,h,k) were no longer observed for 2'-dC-, 2'-F-2'-dC- and 2'-OMe-C-terminated RNAs (Figure S4f,i,l). Compared to the control result for cytosine-terminated RNA (Figure S4c), these cytosine analogue-terminated RNAs did not demonstrate any notable resistance to exonuclease activity (Figure S4f,i,l).

The above results indicate that the structure of the nucleotide analogue at the 3' terminus of RNA plays an essential role in its excision by the SARS-CoV-2 exonuclease complex. In Figure 5, the nucleotide analogues analyzed in this study are ranked in ascending order based on their resistance to exonuclease cleavage in our molecular assay. The nucleotide analogues such as 2'-dN, 2'-OMe-N and 2'-F-2'-dN, where N represents any of the nucleobases tested here, as well as the natural ribonucleotides, when present at the 3' end of RNA, are most easily excised by ExoN. While 2'-NH<sub>2</sub>-2'-dN- and analogues with modifications on the base (Biotin-N and Biotin-2'-dN) provide low resistance to ExoN, 3'-deoxynucleotide analogues (3'-dN and Cidofovir) at the 3' position of the RNA display moderate ExoN resistance. Most importantly, appreciable resistance to ExoN was observed for ddN-, 3'-N<sub>3</sub>-2'-dN-, Tenofovir- and Stavudine-terminated RNAs. These results also indicate that the polarity of the modification group on the sugar ring of the nucleotide analogue attached at the 3' end of the RNA may have an effect on exonuclease cleavage. Nucleotide analogues containing the 2'- and 3'-OH (polar groups) show no resistance towards excision. However, increasing the hydrophobicity at both the 2' and 3' positions of the sugar ring (e.g., ddG, Stavudine and Tenofovir) results in the highest resistance to ExoN excision from RNA.

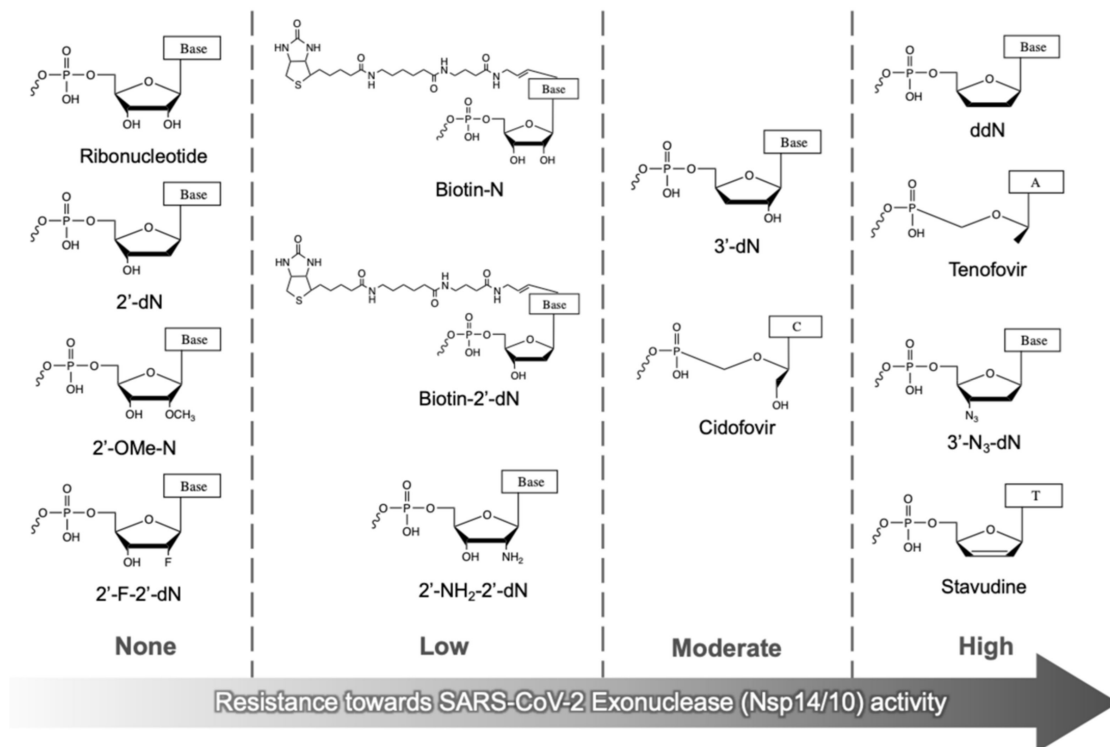


**Figure 5.** Summary of generalized nucleotide analogue structures at the 3' terminus of RNA organized based on their resistance towards SARS-CoV-2 exonuclease activity. The nucleotide analogues fall into four groups showing increasing resistance to ExoN excision from left to right. N indicates any tested nucleobase.

The nucleotide analogues displaying higher resistance to exonuclease excision may help guide the further development of nucleotide analogues with particular structural features for potential coronavirus therapeutics. The ATP analogue Tenofovir-DP, the UTP analogues Stavudine-TP and AZT-TP are obligate terminators of the RdRp extension reaction though less efficiently incorporated than their corresponding natural nucleotides [46,47]. As demonstrated in this work, all three molecules resist excision by the SARS-CoV-2 ExoN to a substantial extent. The dideoxynucleotides also have significant resistance to excision by ExoN. Docking studies performed by Wu et al., indicated that ddA (Didanosine), ddC (Zalcitabine) and Stavudine had comparable binding energies for the active site of SARS-CoV-2 RdRp [68]. The structural modifications identified here will assist in the design of potentially efficient terminators of the RdRp that are also resistant to ExoN. Among the nucleotide analogues we analyzed, even those with substantial resistance to ExoN still showed some excision at longer incubation times. One approach to efficiently inhibit SARS-CoV-2 is the use of combination drug regimens involving distinct RdRp and ExoN inhibitors, as demonstrated in vitro by Wang et al. [41]. Another more challenging option is the development of a single nucleotide analogue that is relatively well incorporated by RdRp and sufficiently resistant to ExoN excision.

**Supplementary Materials:** The following are available online at <https://www.mdpi.com/article/10.3390/v14071413/s1>, Figure S1: Protein sequence conservation in the Nsp10 in representative beta *Coronaviridae* strains, Figure S2: SARS-CoV-2 exonuclease activity with adenosine- or Cordycepin-terminated RNA for different incubation times, Figure S3: SARS-CoV-2 exonuclease activity with uridine analogue-terminated RNA, Figure S4: SARS-CoV-2 exonuclease activity with cytosine- or cytosine analogue-terminated RNA.

**Author Contributions:** Conceptualization, X.W., C.T., I.M., S.K. (Sergey Kalachikov), S.K. (Shiv Kumar), X.L., J.J.R. and J.J.; Experimentation, X.W., C.T., I.M. and S.K. (Sergey Kalachikov); Data analysis, X.W., C.T., I.M., S.K. (Sergey Kalachikov), S.K. (Shiv Kumar), X.L., J.J.R. and J.J.; Writing and Editing, X.W., C.T., I.M., S.K. (Sergey Kalachikov), S.K. (Shiv Kumar), X.L., J.J.R. and J.J. All authors have read and agreed to the published version of the manuscript.

**Funding:** Research reported in this publication was supported by the National Institute of Allergy and Infectious Diseases of the National Institutes of Health under Award Number U19AI171401.

**Institutional Review Board Statement:** Not applicable.

**Informed Consent Statement:** Not applicable.

**Data Availability Statement:** Not applicable.

**Conflicts of Interest:** The authors declare no conflict of interest.

## References

- Zhu, N.; Zhang, D.; Wang, W.; Li, X.; Yang, B.; Song, J.; Zhao, X.; Huang, B.; Shi, W.; Lu, R.; et al. A novel coronavirus from patients with pneumonia in China 2019. *N. Engl. J. Med.* **2020**, *382*, 727–733. [[CrossRef](#)]
- Chen, B.; Tian, E.-K.; He, B.; Tian, L.; Han, R.; Wang, S.; Xiang, Q.; Zhang, S.; El Arnaout, T.; Cheng, W. Overview of lethal human coronaviruses. *Signal Transduct. Target. Ther.* **2020**, *5*, 89. [[CrossRef](#)] [[PubMed](#)]
- Vakulenko, Y.; Deviatkin, A.; Drexler, J.F.; Lukashev, A. Modular evolution of coronavirus genomes. *Viruses* **2021**, *13*, 1270. [[CrossRef](#)] [[PubMed](#)]
- Rodríguez-Román, E.; Gibbs, A.J. Ecology and evolution of betacoronaviruses. In *Coronavirus Disease—COVID-19*; Rezaie, N., Ed.; Springer: Cham, Switzerland, 2021; Volume 1318, pp. 41–60.
- Bai, C.; Zhong, Q.; Gao, G.F. Overview of SARS-CoV-2 genome-encoded proteins. *Sci. China Life Sci.* **2022**, *65*, 280–294. [[CrossRef](#)] [[PubMed](#)]
- Rohaim, M.A.; El Naggari, R.F.; Clayton, E.; Munir, M. Structural and functional insights into non-structural proteins of coronaviruses. *Microb. Pathog.* **2021**, *150*, 104641. [[CrossRef](#)]
- Baddock, H.T.; Brolih, S.; Yosaatmadja, Y.; Ratnaweera, M.; Bielinski, M.; Swift, L.P.; Cruz-Migoni, A.; Fan, H.; Keown, J.R.; Walker, A.P.; et al. Characterization of the SARS-CoV-2 ExoN (nsp14<sup>ExoN</sup>-nsp10) complex: Implications for its role in viral genome stability and inhibitor identification. *Nucleic Acids Res.* **2022**, *50*, 1484–1500. [[CrossRef](#)]
- Saramago, M.; Bária, C.; Costa, V.G.; Souza, C.S.; Viegas, S.C.; Domingues, S.; Lousa, D.; Soares, C.M.; Arraiano, C.M.; Matos, R.G. New targets for drug design: Importance of nsp14/nsp10 complex formation for the 3′–5′ exoribonucleolytic activity on SARS-CoV-2. *FEBS J.* **2021**, *288*, 5130–5147, Epub ahead of print. [[CrossRef](#)] [[PubMed](#)]
- Bouvet, M.; Imbert, I.; Subissi, L.; Gluais, L.; Canard, B.; Decroly, E. RNA 3′-end mismatch excision by the severe acute respiratory syndrome coronavirus nonstructural protein nsp10/nsp14 exoribonuclease complex. *Proc. Natl. Acad. Sci. USA.* **2012**, *109*, 9372–9377. [[CrossRef](#)]
- Gribble, J.; Stevens, L.J.; Agostini, M.L.; Anderson-Daniels, J.; Chappell, J.D.; Lu, X.; Pruijssers, A.J.; Routh, A.L.; Denison, M.R. The coronavirus proofreading exoribonuclease mediates extensive viral recombination. *PLoS Pathog.* **2021**, *17*, e1009226. [[CrossRef](#)]
- Liu, C.; Shi, W.; Becker, S.T.; Schatz, D.G.; Liu, B.; Yang, Y. Structural basis of mismatch recognition by a SARS-CoV-2 proofreading enzyme. *Science* **2021**, *373*, 1142–1146. [[CrossRef](#)]
- Ma, Y.; Wu, L.; Shaw, N.; Gao, Y.; Wang, J.; Sun, Y.; Lou, Z.; Yan, L.; Zhang, R.; Rao, Z. Structural basis and functional analysis of the SARS coronavirus nsp14–nsp10 complex. *Proc. Natl. Acad. Sci. USA* **2015**, *112*, 9436–9441. [[CrossRef](#)] [[PubMed](#)]
- Moeller, N.H.; Shi, K.; Demir, Ö.; Belica, C.; Banerjee, S.; Yin, L.; Durfee, C.; Amaro, R.E.; Aihara, H. Structure and dynamics of SARS-CoV-2 proofreading exoribonuclease ExoN. *Proc. Natl. Acad. Sci. USA* **2022**, *119*, e2106379119. [[CrossRef](#)] [[PubMed](#)]
- Ogando, N.S.; Zevenhoven-Dobbe, J.; van der Meer, Y.; Bredenbeek, P.J.; Posthuma, C.C.; Snijder, E.J. The enzymatic activity of the nsp14 exoribonuclease is critical for replication of MERS-CoV and SARS-CoV-2. *J. Virol.* **2020**, *94*, e01246-20. [[CrossRef](#)]
- Rona, G.; Zeke, A.; Miwatani-Minter, B.; de Vries, M.; Kaur, R.; Schinlever, A.; Garcia, S.F.; Goldberg, H.V.; Wang, H.; Hinds, T.R.; et al. The NSP14/NSP10 RNA repair complex as a pan-coronavirus therapeutic target. *Cell Death Differ.* **2022**, *29*, 285–292. [[CrossRef](#)] [[PubMed](#)]
- Tahir, M. Coronavirus genomic nsp14-ExoN, structure, role, mechanism, and potential application as a drug target. *J. Med. Virol.* **2021**, *93*, 4258–4264. [[CrossRef](#)]
- Robson, F.; Khan, K.S.; Le, T.K.; Paris, C.; Demirbag, S.; Barfuss, P.; Rocchi, P.; Ng, W.-L. Coronavirus RNA proofreading: Molecular basis and therapeutic targeting. *Mol. Cell* **2020**, *79*, 710–727. [[CrossRef](#)]
- Hsu, J.C.-C.; Laurent-Rolle, M.; Pawlak, J.B.; Wilen, C.B.; Cresswell, P. Translational shutdown and evasion of the innate immune response by SARS-CoV-2 NSP14 protein. *Proc. Natl. Acad. Sci. USA* **2021**, *118*, e2101161118. [[CrossRef](#)]

19. Gao, Y.; Yan, L.; Huang, Y.; Liu, F.; Zhao, Y.; Cao, L.; Wang, T.; Sun, Q.; Ming, Z.; Zhang, Y.; et al. Structure of the RNA-dependent RNA polymerase from COVID-19 virus. *Science* **2020**, *368*, 779–782. [[CrossRef](#)]
20. Hillen, H.S.; Kokic, G.; Farnung, L.; Dienemann, C.; Tegunov, D.; Cramer, P. Structure of replicating SARS-CoV-2 polymerase. *Nature* **2020**, *584*, 154–156. [[CrossRef](#)]
21. Wang, Q.; Wu, J.; Wang, H.; Gao, Y.; Liu, Q.; Mu, A.; Ji, W.; Yan, L.; Zhu, Y.; Zhu, C.; et al. Structural basis for RNA replication by the SARS-CoV-2 polymerase. *Cell* **2020**, *182*, 417–428. [[CrossRef](#)]
22. Yin, W.; Mao, C.; Luan, X.; Shen, D.-D.; Shen, Q.; Su, H.; Wang, X.; Zhou, F.; Zhao, W.; Gao, M.; et al. Structural basis for inhibition of the RNA-dependent RNA polymerase from SARS-CoV-2 by remdesivir. *Science* **2020**, *368*, 1499–1504. [[CrossRef](#)] [[PubMed](#)]
23. Kokic, G.; Hillen, H.S.; Tegunov, D.; Dienemann, C.; Seitz, F.; Schmitzova, J.; Farnung, L.; Siewert, A.; Hobartner, C.; Cramer, P. Mechanism of SARS-CoV-2 polymerase stalling by remdesivir. *Nat. Commun.* **2021**, *12*, 279. [[CrossRef](#)] [[PubMed](#)]
24. Naydenova, K.; Muir, K.W.; Wu, L.-F.; Zhang, Z.; Coscia, F.; Peet, M.J.; Castro-Hartmann, P.; Qian, P.; Sader, K.; Dent, K.; et al. Structure of the SARS-CoV-2 RNA-dependent RNA polymerase in the presence of favipiravir-RTP. *Proc. Natl. Acad. Sci. USA* **2021**, *118*, e2021946118. [[CrossRef](#)] [[PubMed](#)]
25. Lin, S.; Chen, H.; Chen, Z.; Yang, F.; Ye, F.; Zheng, Y.; Yang, J.; Lin, X.; Sun, H.; Wang, L.; et al. Crystal structure of SARS-CoV-2 nsp10 bound to nsp14-ExoN domain reveals an exoribonuclease with both structural and functional integrity. *Nucleic Acids Res.* **2021**, *49*, 5382–5392. [[CrossRef](#)]
26. Yan, L.; Zhang, Y.; Ge, J.; Zheng, L.; Gao, Y.; Wang, T.; Jia, Z.; Wang, H.; Huang, Y.; Li, M.; et al. Architecture of a SARS-CoV-2 mini replication and transcription complex. *Nat. Commun.* **2020**, *11*, 5874. [[CrossRef](#)]
27. Yan, L.; Ge, J.; Zheng, L.; Zhang, Y.; Gao, Y.; Wang, T.; Huang, Y.; Yang, Y.; Gao, S.; Li, M.; et al. Cryo-EM structure of an extended SARS-CoV-2 replication and transcription complex reveals an intermediate state in cap synthesis. *Cell* **2021**, *184*, 184–193. [[CrossRef](#)]
28. Yan, L.; Yang, Y.; Li, M.; Zhang, Y.; Zheng, L.; Ge, J.; Huang, Y.C.; Liu, Z.; Wang, T.; Gao, S.; et al. Coupling of N7-methyltransferase and 30-50 exoribonuclease with SARS-CoV-2 polymerase reveals mechanisms for capping and proofreading. *Cell* **2021**, *184*, 3474–3485. [[CrossRef](#)]
29. Chen, J.; Malone, B.; Llewellyn, E.; Grasso, M.; Shelton, P.M.M.; Olinares, P.D.B.; Maruthi, K.; Eng, E.T.; Vatandaslar, H.; Chait, B.T.; et al. Structural basis for helicase-polymerase coupling in the SARS-CoV-2 replication-transcription complex. *Cell* **2020**, *182*, 1560–1573. [[CrossRef](#)]
30. Malone, B.; Chen, J.; Wang, Q.; Llewellyn, E.; Choi, Y.J.; Olinares, P.D.B.; Cao, X.; Hernandez, C.; Eng, E.T.; Chait, B.T.; et al. Structural basis for backtracking by the SARS-CoV-2 replication-transcription complex. *Proc. Natl. Acad. Sci. USA* **2021**, *118*, e2102516118. [[CrossRef](#)]
31. Subissi, L.; Posthuma, C.C.; Collet, A.; Zevenhoven-Dobbe, J.C.; Gorbalenya, A.E.; Decroly, E.; Snijder, E.J.; Canard, B.; Imbert, I. One severe acute respiratory syndrome coronavirus protein complex integrates processive RNA polymerase and exonuclease activities. *Proc. Natl. Acad. Sci. USA* **2014**, *111*, E3900–E3909. [[CrossRef](#)]
32. Ogando, N.S.; Ferron, F.; Decroly, E.; Canard, B.; Posthuma, C.C.; Snijder, E.J. The curious case of the Nidovirus exoribonuclease: Its role in RNA synthesis and replication fidelity. *Front. Microbiol.* **2019**, *10*, 813. [[CrossRef](#)] [[PubMed](#)]
33. Romano, M.; Ruggiero, A.; Squeglia, F.; Maga, G.; Berisio, R. A structural view of SARS-CoV-2 RNA replication machinery: RNA synthesis, proofreading and final capping. *Cells* **2020**, *9*, 1267. [[CrossRef](#)]
34. Eskier, D.; Suner, A.; Oktay, Y.; Karakulah, G. Mutations of SARS-CoV-2 nsp14 exhibit strong association with increased genome-wide mutation load. *PeerJ* **2020**, *8*, e10181. [[CrossRef](#)] [[PubMed](#)]
35. Ogando, N.S.; El Kazzi, P.; Zevenhoven-Dobbe, J.C.; Bontes, B.W.; Decombe, A.; Posthuma, C.C.; Thiel, V.; Canard, B.; Ferron, F.; Decroly, E.; et al. Structure-function analysis of the nsp14 N7-guanine methyltransferase reveals an essential role in *Betacoronavirus* replication. *Proc. Natl. Acad. Sci. USA* **2021**, *49*, e2108709118. [[CrossRef](#)]
36. Niu, X.; Kong, F.; Hou, Y.J.; Wang, Q. Crucial mutation in the exoribonuclease domain of nsp14 of PEDV leads to high genetic instability during viral replication. *Cell Biosci.* **2021**, *11*, 106. [[CrossRef](#)] [[PubMed](#)]
37. Bouvet, M.; Lugari, A.; Posthuma, C.C.; Zevenhoven, J.C.; Bernard, S.; Betzi, S.; Imbert, I.; Canard, B.; Guillemot, J.-C.; Lécine, P.; et al. Coronavirus nsp10, a critical co-factor for activation of multiple replicative enzymes. *J. Biol. Chem.* **2014**, *289*, 25783–25796. [[CrossRef](#)]
38. Keep, S.; Stevenson-Leggett, P.; Dowgier, G.; Everest, H.; Freimanis, G.; Oade, M.; Hammond, J.A.; Armesto, M.; Vila, R.; Bru, T.; et al. Identification of amino acids within nonstructural proteins 10 and 14 of the avian coronavirus infectious bronchitis virus that result in attenuation *In Vivo* and *In Ovo*. *J. Virol.* **2022**, *96*, e02059-21. [[CrossRef](#)]
39. Jockusch, S.; Tao, C.; Li, X.; Chien, M.; Kumar, S.; Morozova, I.; Kalachikov, S.; Russo, J.J.; Ju, J. Sofosbuvir terminated RNA is more resistant to SARS-CoV-2 proofreader than RNA terminated by Remdesivir. *Sci. Rep.* **2020**, *10*, 16577. [[CrossRef](#)]
40. Canal, B.; McClure, A.W.; Curran, J.F.; Wu, M.; Ulferts, R.; Weissman, F.; Zeng, J.; Bertolin, A.P.; Milligan, J.C.; Basu, S.; et al. Identifying SARS-CoV-2 antiviral compounds by screening for small molecule inhibitors of nsp14/nsp10 exoribonuclease. *Bi-ohem. J.* **2021**, *478*, 2445–2564. [[CrossRef](#)]
41. Wang, X.; Sacramento, C.Q.; Jockusch, S.; Chaves, O.A.; Tao, C.; Fintelman-Rodrigues, N.; Chien, M.; Temerozo, J.R.; Li, X.; Kumar, S.; et al. Combination of antiviral drugs inhibits SARS-CoV-2 polymerase and exonuclease and demonstrates COVID-19 therapeutic potential in viral cell culture. *Commun. Biol.* **2022**, *5*, 154. [[CrossRef](#)]

42. Gordon, C.J.; Tchesnokov, E.P.; Woolner, E.; Perry, J.K.; Feng, J.Y.; Porter, D.P.; Götte, M. Remdesivir is a direct-acting antiviral that inhibits RNA-dependent RNA polymerase from severe acute respiratory syndrome coronavirus 2 with high potency. *J. Biol. Chem.* **2020**, *295*, 6785–6797. [[CrossRef](#)] [[PubMed](#)]
43. Bravo, J.P.K.; Dangerfield, T.L.; Taylor, D.W.; Johnson, K.A. Remdesivir is a delayed translocation inhibitor of SARS-CoV-2 replication. *Mol. Cell* **2021**, *81*, 1548–1552. [[CrossRef](#)] [[PubMed](#)]
44. Vicenti, I.; Zazzi, M.; Saladini, F. SARS-CoV-2 RNA-dependent RNA polymerase as a therapeutic target for COVID-19. *Expert Opin. Ther. Pat.* **2021**, *31*, 325–337. [[CrossRef](#)] [[PubMed](#)]
45. Seifert, M.; Bera, S.C.; van Nies, P.; Kirchdoerfer, R.N.; Shannon, A.; Le, T.-T.-N.; Meng, X.; Xia, H.; Wood, J.M.; Harris, L.D.; et al. Inhibition of SARS-CoV-2 polymerase by nucleotide analogs from a single-molecule perspective. *eLife* **2021**, *10*, e70968. [[CrossRef](#)]
46. Chien, M.; Anderson, T.K.; Jockusch, S.; Tao, C.; Li, X.; Kumar, S.; Russo, J.J.; Kirchdoerfer, R.N.; Ju, J. Nucleotide analogues as inhibitors of SARS-CoV-2 polymerase, a key drug target for COVID-19. *J. Proteome Res.* **2020**, *19*, 4690–4697. [[CrossRef](#)]
47. Jockusch, S.; Tao, C.; Li, X.; Anderson, T.K.; Chien, M.; Kumar, S.; Russo, J.J.; Kirchdoerfer, R.N.; Ju, J. A library of nucleotide analogues terminate RNA synthesis catalyzed by polymerases of coronaviruses that cause SARS and COVID-19. *Antivir. Res.* **2020**, *180*, 104857. [[CrossRef](#)]
48. Blasiak, A.; Lim, J.J.; Seah, S.G.K.; Kee, T.; Remus, A.; Chye, D.H.; Wong, P.S.; Hooi, L.; Truong, A.T.L.; Le, N.; et al. IDentif.AI: Rapidly optimizing combination therapy design against severe Acute Respiratory Syndrome Coronavirus 2 (SARS-CoV-2) with digital drug development. *Bioeng. Transl. Med.* **2020**, *6*, e10196. [[CrossRef](#)]
49. Dejmeek, M.; Konkol'ová, E.; Eyer, L.; Straková, P.; Svoboda, P.; Šála, M.; Krejčová, K.; Růžek, D.; Boura, E.; Nencka, R. Non-nucleotide RNA-dependent RNA polymerase inhibitor that blocks SARS-CoV-2 replication. *Viruses* **2021**, *13*, 1585. [[CrossRef](#)]
50. Yang, H.; Rao, Z. Structural biology of SARS-CoV-2 and implications for therapeutic development. *Nat. Rev. Microbiol.* **2021**, *19*, 685–700. [[CrossRef](#)]
51. Minskaia, E.; Hertzog, T.; Gorbalenya, A.E.; Campanacci, V.; Cambillau, C.; Canard, B.; Ziebhur, J. Discovery of an RNA virus 3'→5' exoribonuclease that is critically involved in coronavirus RNA synthesis. *Proc. Natl. Acad. Sci. USA* **2006**, *103*, 5108–5113. [[CrossRef](#)]
52. Gitto, S.; Gamal, N.; Andreone, P. NS5A inhibitors for the treatment of hepatitis C infection. *J. Viral Hepat.* **2017**, *24*, 180–186. [[CrossRef](#)] [[PubMed](#)]
53. Sacramento, C.Q.; Fintelman-Rodrigues, N.; Temerozo, J.R.; de Paul Dias Da Silva, A.; da Silva Gomes Dias, S.; dos Santos da Silva, C.; Ferreira, A.C.; Mattos, M.; Pão, C.R.R.; de Freitas, C.S.; et al. *In vitro* antiviral activity of the anti-HCV drugs daclatasvir and sofosbuvir against SARS-CoV-2, the aetiological agent of COVID-19. *J. Antimicrob. Chemother.* **2021**, *76*, 1874–1885. [[CrossRef](#)] [[PubMed](#)]
54. Sanders, R. Can Hepatitis C Drugs Help Remdesivir Fight COVID-19? Available online: <https://news.berkeley.edu/2021/02/03/can-hepatitis-c-drugs-help-remdesivir-fight-covid-19/> (accessed on 20 May 2022).
55. Khater, S.; Kumar, P.; Dasgupta, N.; Das, G.; Ray, S.; Prakash, A. Combining SARS-CoV-2 proofreading exonuclease and RNA-dependent RNA polymerase inhibitors as a strategy to combat COVID-19: A high-throughput in silico screen. *Front. Microbiol.* **2021**, *12*, 647693. [[CrossRef](#)] [[PubMed](#)]
56. Nguyenla, X.; Wehri, E.; Van Dis, E.; Biering, S.B.; Yamashiro, L.H.; Stroumza, J.; Dugast-Darzacq, C.; Graham, T.; Stanley, S.; Schaletzky, J. Discovery of SARS-CoV-2 antiviral synergy between remdesivir and approved drugs in human lung cells. *bioRxiv* **2020**. [[CrossRef](#)]
57. Chen, Z.; Azman, A.S.; Chen, X.; Zou, J.; Tian, Y.; Sun, R.; Xu, X.; Wu, Y.; Lu, W.; Ge, S.; et al. Global landscape of SARS-CoV-2 genomic surveillance and data sharing. *Nat. Genet.* **2022**, *54*, 499–507. [[CrossRef](#)] [[PubMed](#)]
58. Fan, L.; Hu, X.; Chen, Y.; Peng, X.; Fu, Y.; Zheng, Y.; Yu, J.; He, J. Biological significance of the genome variation and structural dynamics of SARS-CoV-2 B.1.617. *Front. Microbiol.* **2021**, *12*, 750725. [[CrossRef](#)] [[PubMed](#)]
59. Wiegand, T.; McVey, A.; Nemudraia, A.; Nemudryi, A.; Wiedenheft, A. The rise and fall of SARS-CoV-2 variants and the mutational profile of Omicron. *bioRxiv* **2021**. [[CrossRef](#)]
60. Jung, C.; Kmiec, D.; Koepke, L.; Zech, F.; Jacob, T.; Sparrer, K.M.J.; Kirchhoff, F. Omicron: What makes the latest SARS-CoV-2 variant of concern so concerning? *J. Virol.* **2022**, *96*, e02077-21. [[CrossRef](#)]
61. Hadfield, J.; Megill, C.; Bell, S.M.; Huddleston, J.; Potter, B.; Callender, C.; Sagulenko, P.; Bedford, T.; Neher, R.A. Nextstrain: Real-time tracking of pathogen evolution. *Bioinformatics* **2018**, *34*, 4121–4123. [[CrossRef](#)]
62. Sievers, F.; Wilm, A.; Dineen, D.; Gibson, T.J.; Karplus, K.; Li, W.; Lopez, R.; McWilliam, H.; Remmert, M.; Söding, J.; et al. Fast, scalable generation of high-quality protein multiple sequence alignments using Clustal Omega. *Mol. Syst. Biol.* **2011**, *7*, 539. [[CrossRef](#)]
63. Madeira, F.; Pearce, M.; Tivey, A.R.N.; Basutkar, P.; Lee, J.; Edbali, O.; Madhusoodanan, N.; Kolesnikov, A.; Lopez, R. Search and sequence analysis tools services from EMBL-EBI in 2022. *Nucleic Acids Res.* **2022**. *online ahead of print*. [[CrossRef](#)] [[PubMed](#)]
64. Brown, N.P.; Leroy, C.; Sander, C. MView: A web-compatible database search or multiple alignment viewer. *Bioinformatics* **1998**, *14*, 380–381. [[CrossRef](#)] [[PubMed](#)]
65. Smith, E.C.; Case, J.B.; Blanc, H.; Isakov, O.; Shomron, N.; Vignuzzi, M.; Denisonon, M.R. Mutations in coronavirus nonstructural protein 10 decrease viral replication fidelity. *J. Virol.* **2015**, *89*, 6418–6426. [[CrossRef](#)] [[PubMed](#)]
66. Rabie, A.M. Potent inhibitory activities of the adenosine analogue cordycepin on SARS-CoV-2 replication. *ACS Omega* **2022**, *7*, 2960–2969. [[CrossRef](#)]

- 
67. Arnold, J.J.; Sharma, S.D.; Feng, J.Y.; Ray, A.S.; Smidansky, E.D.; Kireeva, M.L.; Cho, A.; Perry, J.; Vela, J.E.; Park, Y.; et al. Sensitivity of mitochondrial transcription and resistance of RNA polymerase II dependent nuclear transcription to antiviral ribonucleosides. *PLoS Pathog.* **2012**, *8*, e1003030. [[CrossRef](#)]
  68. Wu, Y.; Chang, K.Y.; Lou, L.; Edwards, L.G.; Doma, B.K.; Xie, Z.R. In silico identification of drug candidates against COVID-19. *Inform. Med. Unlocked* **2020**, *21*, 100461. [[CrossRef](#)]